Chinese Journal of Structural Chemistry

ARTICLE

A Water-Stable 3D Eu(III)-Organic Framework as a Bi-Functional Ratiometric Luminescent Sensor for Fast, Sensitive and Selective Detection of ODZ and Hg^{2+} in Aqueous Media

Xiuting Gao[1], Nana Chen[1], Minglei Cao[2], Yang Shi[1] and Qingfu Zhang[1]*

[1]*College of Chemistry and Chemical Engineering, Liaocheng University, Liaocheng, Shandong 252059, China*
[2]*Shandong Ruijie New Material Co.Ltd, Liaocheng, Shandong 252000, China*

ABSTRACT The fast, sensitive and selective detection of some antibiotics and heavy metal cations in water is highly desirable for environmental protection and human health, but it is still currently challenging. In this work, a new luminescent Eu(III)-based metal-organic framework (MOF), $\{[(CH_3)_2NH_2][Eu(L)_2(H_2O)_2]\cdot xDMF\}_n$ (**1**) [H_2L = 4,4'-((naphthalene-1,4-dicarbonyl)bis(azanediyl))dibenzoic acid], was solvothermally synthesized. Complex **1** exhibits good water stability and luminescent property and could serve as a bi-functional ratiometric luminescent sensor for fast, sensitive and selective detection of ornidazole (ODZ) and Hg^{2+} in aqueous solution. The corresponding luminescent mechanism has also been discussed. This work indicates that **1** as a promising luminescent material exhibits luminescent quenching behavior for ODZ and luminescent enhancement behavior for Hg^{2+} in H_2O, which will promote the practical application of Ln-MOF-based ratiometric luminescent sensors in monitoring antibiotics and metal ions pollutants in the environmental water matrices.

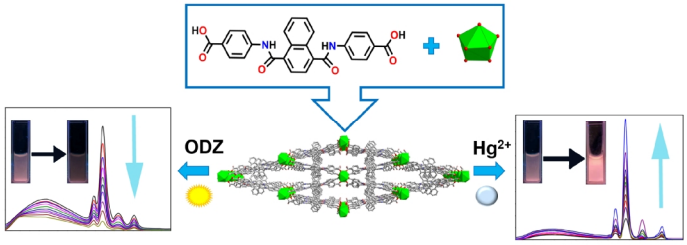

Keywords: lanthanide MOF, ratiometric luminescent sensor, water-stability, antibiotics, metal ions

n INTRODUCTION

With the development of economy, people have higher demand for their health. Antibiotics are important pharmaceuticals and widely used for the prevention of infections by bacteria and fungi.[1,2] However, the abuse of antibiotics has brought various problems, which can give rise to adverse effects on nontarget organisms, increase bacterial resistance and bright serious ecological environmental pollution.[3,4] Mercury (Hg^{2+}) as an extremely toxic metal ion released from industry is one of the most environmental pollutants. It has shown an extensive range of poisonous actions to human and the accumulation of Hg^{2+} in human body leads to several diseases such as neurodevelopmental disorders and subclinical brain dyfunction.[5] In addition, antibiotics and Hg^{2+} would constantly enter aquatic systems through anthropogenic emissions over time. Therefore, it is a significantly urgent requirement to develop an effective method for sensing these harmful pollutants in water.

The current detection methods, such as liquid chromatography-tandem mass spectrometry (LC-MS),[6] ion mobility spectrometry (IMS),[7] capillary electrophoresis (CE),[8] and capillary electrochromatography coupled to mass spectrometry (CEC-MS),[9] are usually time-consuming, expensive, and complex operation. Compared with these methods, luminescent method has been considered as one of the promising and compelling techniques for sensing antibiotics and metal ions due to fast response, cost-effective and convenient analysis. The choice of sensor material is central to achieving an effective detection of the targeted analyte. Until now, several inorganic luminescent nanoprobes have been reported.[10-12] Compared with these inorganic materials, MOFs as prospective fluorescent sensing materials have attracted more attention due to their unique properties such as permanent porosity, high surface area, and easily tailorable structures and functions.[13-15] A number of luminescent MOFs with a single emission center have been used to detect different analytes,[16,17] but such monochromatic luminescence signals are not accurate because many non-analyte factors such as unstable instrumental parameters and background luminescence can alter the absolute solid-state luminescence intensities.[18] In contrast, ratiometric luminescent sensors based on the intensity ratio of two independent emissions can solve the problem mentioned because the self-calibrating or self-referencing mechanism from different but correlated emission centers can minimize the external influence.[19-22] Therefore, the ratiometric luminescent sensors have better accuracies, sensitivities, and selectivities toward environmental pollutants.

Luminescent lanthanide metal-organic frameworks (Ln-MOFs) with fascinating optical properties, such as large Stokes shifts, high color purity, relatively long luminescence lifetimes and narrow emission spectra, have recently been demonstrated as a promising strategy for constructing ratiometric luminescent sensors.[23,24] Up to now, many MOF-based ratiometric sensors have been reported, which were achieved by encapsulating Ln^{3+}, dyes, carbon dots (CDs), and luminescent complexes as luminescent modules into luminescent MOFs.[25] Qian *et al*. first encapsulated the luminescent lanthanide metal ion Eu^{3+} in the metal-organic framework UiO-66-$(COOH)_2$ crystal and then introduced the transition metal ion Cu^{2+}, thus obtaining a new ratiometric lumine-

DOI: 10.14102/j.cnki.0254-5861.2022-0171

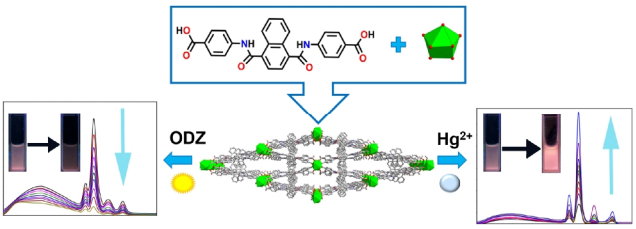

Figure 1. Schematic diagram of luminescent MOF **1** as a bi-responsive chemical sensor for detecting ODZ and Hg^{2+} in water.

scent sensor Eu^{3+}/Cu^{2+}@UiO-66-$(COOH)_2$ for detecting H_2S content in aqueous solution.[26] Hou *et al*. have reported several mixed lanthanide metal-organic frameworks Ln (TATB) for visual detection of fluoride anions.[27] Xiao and coworkers prepared lanthanide metal-organic framework Eu-dipicolinic acid/2-aminophthalic acid (Eu-DPA/PTA-NH_2) as a double-color ratiometric fluorescent water sensor, which showed ultrasensitive and linear broad-range response to water.[28] However, the MOF synthesized by assembly is complex and lacks long-term stability.

In this work, we elaborately designed and successfully synthesized an acylamide-functionalized dicarboxylate ligand 4,4′-((naphthalene-1,4-dicarbonyl)bis(azanediyl))dibenzoic acid (H_2L), in which two acylamide groups are introduced as guest-accessible functional organic sites (FOS) to promote the sensing ability of target MOFs. As expected, a new Eu(III)-MOF {$[(CH_3)_2NH_2][Eu(L)_2(H_2O)_2]\cdot xDMF$}$_n$ (**1**) was synthesized by the reaction of H_2L and $Eu(NO_3)_3\cdot 6H_2O$ under solvothermal conditions. The analysis showed that complex **1** exhibits a 3D porous structure with good water stability and luminescent property, so it could be used as a ratiometric luminescent sensor for rapid, sensitive, selective and reversible detecting ornidazole (ODZ) and Hg^{2+} in aqueous media (Figure 1). To our knowledge, no MOFs as a ratiometric luminescent sensor via the quenching and enhancement of its luminescence for ornidazole and Hg^{2+} detection have been reported so far.

n RESULTS AND DISCUSSION

Description of the Crystal Structure. Single-crystal X-ray diffraction analysis reveals that complex **1** crystallizes in orthorhombic space group *Pcc*2 and represents a 3D framework based on L^{2-} ligands and the [EuO_8] building block. As shown in Figure 2a, each central Eu(III) ion is eight-coordinated by four carboxylate oxygens from four μ_4-η^1:η^1:η^1:η^1 bridging L^{2-} ligands, two carboxylate oxygens from two μ_2-η^1:η^1 bridging L^{2-} ligands and two water oxygen atoms. The coordination geometry for Eu1 was biaugmented trigonal prism with the CShM value of 0.901, whereas Eu2 adopts a biaugmented trigonal dodecahedral geometry with CShM in 0.932, as calculated by SHAPE 2.1.[29] The Eu-O bond lengths (2.304(9)-2.526(10) Å) fall in a normal range. In complex **1**, two adjacent Eu^{3+} ions were connected by carboxylate groups from L^{2-} ligands to produce the 1D parallelly aligned Eu-O-C chains extending along the c axis with the Eu···Eu separation of 4.9475(29) Å (Figure 2b). As shown in Figure 2c, adjacent Eu-O-C chains are linked by two L^{2-} ligands to form a 2D layer, and then these 2D layers are connected by another L^{2-} ligands, forming a three-dimensional bcu type structure (Figure 2d), with 1D channels of rhombic apertures in the [001] direction. In general, **1** was connected by ligands and [EuO_8] building block to form a 3D porous anionic framework. Negative charges of the framework were balanced by protonated $(CH_3)_2NH_2^+$ ions generated upon the hydrolysis of DMF molecules under solvothermal conditions.[30,31] The guest $(CH_3)_2NH_2^+$ cations and solvent molecules were seriously disordered and removed by the SQUEEZE routine in PLATON. In addition, PLATON analysis reveals that the 3D porous structure is composed of large voids of 1497.8 $Å^3$ that represents approximately 26.9% per unit cell volume without guest molecules.[32]

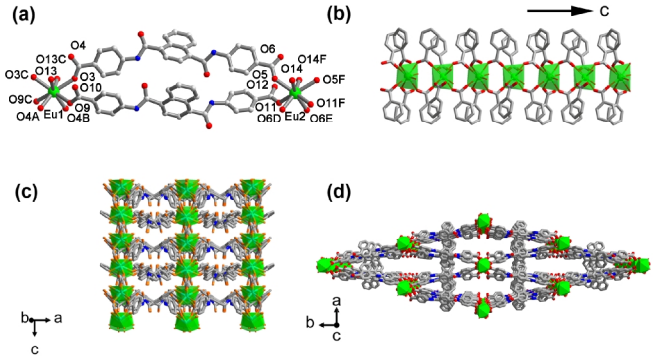

Figure 2. (a) Coordination environments of the metal ion in Eu-MOF. All hydrogen atoms and dimethylammonium cations were omitted for clarity. (b) The 1D Eu-O-C chain extending along the c axis. (c) 2D layer of **1**. (d) 3D framework of **1**.

Stability of 1. Considering the practical application in aqueous media, the water stability of complex **1** was further investigated and a series of experiments were carried out. PXRD measurements for **1** immersed in water at room temperature for 72 h, boiling water for 24 h, HCl (pH = 4) and NaOH (pH = 10) solutions at room temperature for 72 h were carried out, respectively. All the PXRD patterns are consistent with that of pristine **1**, revealing its good water stability (Figure 3a). In addition, the hydrophilic/hydrophobic properties of **1** were investigated by water contact angle measurements. As shown in Figure 3b, complex **1** exhibits slightly hydrophilic property with a water contact angle of about 82°, which may be due to the existence of strong hydrophilic acylamide group and the hydrophobic aromatic group of L^{2-} ligand in **1**. This result is similar to that observed in our previously reported work.[33,34]

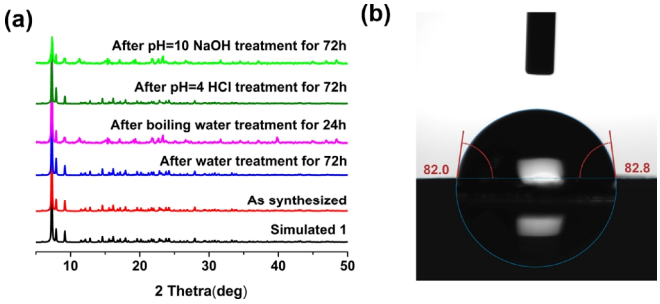

Figure 3. (a) PXRD patterns of **1** after different treatments. (b) Water contact angle in **1**.

Chin. J. Struct. Chem. **2022**, 41, 2211110-2211116
DOI: 10.14102/j.cnki.0254-5861.2022-0171

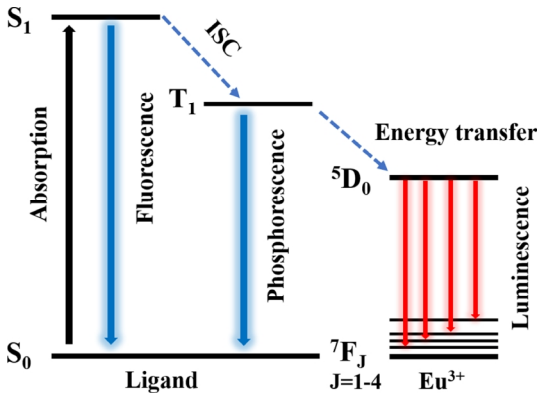

Scheme 1. Schematic of the energy-transfer process of MOF in this work. (ISC: intersystem crossing process)

Therefore, the good water stability of MOF showed great potential for developing luminescent probe in aqueous media.

Luminescent Property. The luminescence properties of **1** and H_2L ligand dispersed in water were investigated at room temperature. The H_2L ligand displayed luminescence centered around 413 nm when excited by 326 nm (Figure S1). After incorporating Eu^{3+} cations, the ligand-centered (LC) emission exhibited a broad emission band at 467 nm and the luminous intensity of LC decreased significantly. In addition, the characteristic narrow bands of the Eu^{3+} ion appear at 591, 619, 662 and 698 nm ascribed to the $^5D_0 \rightarrow {}^7F_J$ (J = 1, 2, 3 and 4, respectively) transition (λ_{ex} = 326 nm). The diminished LC emission in MOF **1** and the strong red luminescence under UV-light irradiation (inset of Figure S1) indicate that there is "antenna effect"[35] (Energy migration takes place upon ligand absorption, followed by intersystem crossing $S_1 \rightarrow T_1$ and antenna $T_1 \rightarrow$ f transfer, and then generates f-f emission of Ln^{3+}) in MOF luminescence process (Scheme 1). Considering the remarkable luminescence properties of **1** in the visible region, we investigated its potential application as a photoluminescence sensing material. It is worth noting that the fluorescence intensity of **1** suspension at 619 nm showed negligible change after standing for 7 days, indicating good day-to-day fluorescence stability in aqueous solution (Figure S2).

Selective Sensing of Antibiotics. Considering the good water stability and luminescent property, we investigated the sensing ability of **1** for different antibiotics. It is noteworthy that two emission peaks at 467 (ligand-centered emission) and 619 nm (Eu^{3+} emission) are relatively far apart, showing different response behaviors to various antibiotics in water. In this work, the luminescence sensing experiments for different antibiotics, including ornidazole (ODZ), cefixime (CFX), sulfadiazine (SDZ), florfenicol (FFC), cefradine (CFD), penicillin (PCL), amoxicillin (ACL), sulfamethazine (SMZ) and thiamphenicol (THI), were carried out in aqueous media (Figure S3). As shown in Figure 4a, different antibiotics exhibit different luminescent quenching efficiency toward **1**. The ODZ displays the highest quenching efficiency up to 90%. The quenching efficiencies of **1** follow the order of ODZ > CFX > SDZ > SMZ > FFC > PCL > CFD > ACL> THI (Figure 4a), suggesting it can be used as a potential luminescent sensor for highly selective recognition of ODZ.

To further investigate the detection ability of **1** in detail, luminescence titration experiments were conducted. As shown in Figure 4b, the dual-emission peaks of **1** all decrease with increasing the concentration of ODZ, where slight changes in emission intensity at 467 nm and great changes in emission intensity at 619 nm were observed. Thus, the luminescence intensity ratio (I_{619}/I_{467}) of Eu^{3+} and the ligand center was used as the output signal and complex **1** as ratiometric fluorescence probe for the detection of ODZ. As shown in Figure 4c, the reduction coefficients K_{SV} for ODZ can be calculated by the Stern-Völmer (S-V) equation:[36] $I_{0R}/I_R = K_{SV}[A] + 1$, where [A] represents the molar concentration of antibiotics and I_{0R} and I_R are defined as the luminescence intensity ratios in the absence and presence of antibiotics, respectively, which are used to replace the absolute luminescence intensity (I_0 and I, respectively) in the above equation.[37] A good linear response was observed between the ratio of I_{619}/I_{467} and the concentration of ODZ at low concentrations, but the relationship becomes nonlinear at higher concentrations. The nonlinear SV plot at high concentrations should be ascribed to self-absorption and/or an energy-transfer process.[33,38] The K_{SV} value for ODZ is 2.43×10^3 M^{-1}. The limit of detection (LOD = 3σ/k, where σ is the standard deviation for five blank measurements and k is the slope of the calibration curve) for ODZ is 0.15 μM, which is lower than some of other MOFs (Table S3). The low LOD shows the highly sensitive sensing ability of **1** toward ODZ. To study the possible influence of other matters in the multicontaminant system, the competition experiments were performed with the coexistence of ODZ and other different antibiotics in water. As shown in Figure 4d, the emission intensity of **1** was not affected in the presence of other antibiotics, which indicated that the interference from other antibiotics could be neglected and confirmed the highly selective detecting ability of **1** toward ODZ.

The response time and recyclability of a sensor material are also important factors for practical applications. First, the re-

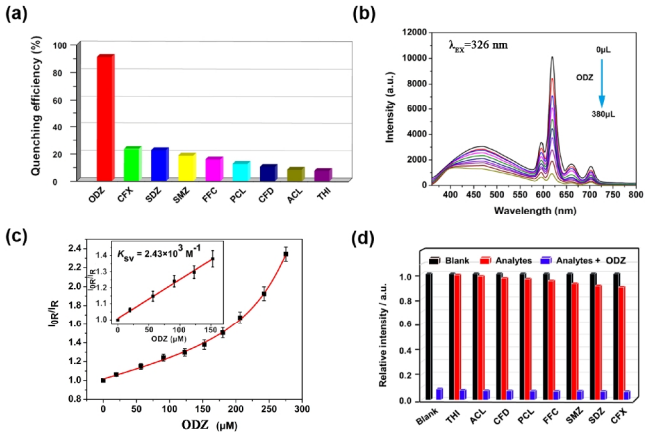

Figure 4. (a) Luminescence quenching efficiency for **1** dispersed in different antibiotics when excited under excitation at 326 nm. (b) Luminescent emission spectra of **1** (10^{-3} M) upon incremental addition of ODZ (10^{-3} M) under excitation at 326 nm. (c) SV plot of ODZ. Inset: SV plot at lower concentration under excitation at 326 nm. (d) The fluorescence emissive response of **1** for detecting ODZ in the presence of other interfering antibiotics.

DOI: 10.14102/j.cnki.0254-5861.2022-0171

sponse kinetics of the probe toward ODZ was investigated. Upon the addition of 380 μL of ODZ, the fluorescence intensity of MOF **1** at 619 nm was measured with different response time. As shown in Figure S4, after adding ODZ, the fluorescence of **1** is quickly quenched by exposure to ODZ for 30 s and reach the minimum value after 2 min. The result indicated the rapid response capability of MOF **1**. It is noteworthy that complex **1** could be regenerated and reused by centrifuging the dispersed suspension after sensing and washing several times with water. As shown in Figure S5, the fluorescence intensities of **1** could still be almost restored to its original level even after five cycles, which suggests good its recyclability. These experiments testified that **1** can be used as fast, selective, sensitive and recyclable luminescent sensor toward ODZ in aqueous solution.

To understand the highly sensitive and selective ODZ detection process better, the quenching mechanism of **1** was investigated. As shown in Figure S6, the PXRD patterns are almost the same as the as-synthesized **1** after five cyclic experiments, implying the luminescence quenching is not caused by collapse of the framework. In addition, the luminescent lifetime of **1** was also tested before and after the addition of antibiotic. As shown in Figure S7, the luminescence lifetime of **1** remains almost unchanged after adding ODZ, which suggested no strong interactions between the antibiotic and **1**. Therefore, the possible sensing mechanism may be attributed to photoinduced electron transfer (PET) between the ligands and the analyte molecules. In PET process, the lower the unoccupied molecular orbital (LUMO) energy is, the higher the electron accepting ability of the analytes will be.

As revealed in Figure 5a and Table S4, the HOMO and LUMO orbital energies of electron-deficient antibiotics, as calculated by DFT method at the B3LYP/6-31G* level, are in good agreement with the maximum quenching efficiency observed for ODZ, but the LUMO energy trend of all antibiotics is different from the sequence of the observed quenching efficiency. The result implies that PET is not the only reason for luminescence quenching in the current system. As shown in Figure 5b, the absorption spectrum of ODZ has the greatest degree of overlapping with the excitation spectrum of **1**. The competitive absorption of the excitation energy between antibiotics and MOF might be another reason for the luminescent quenching.[38] The excitation energy of MOF was partially absorbed by analyte, which reduced the energy transfer efficiency from H_2L to Eu^{3+} and caused the fluorescence quenching. Consequently, PET and the competitive absorption of the light source energy simultaneously exist between MOF and antibiotics, which leads to high luminescence quenching.

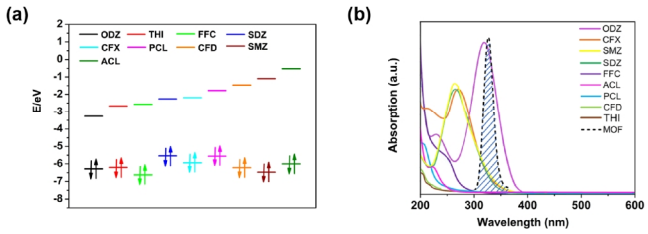

Figure 5. (a) HOMO and LUMO energies for antibiotics arranged in descending order of LUMO energies. (b) The absorption spectra of selected antibiotics and excitation of **1** in 326 nm.

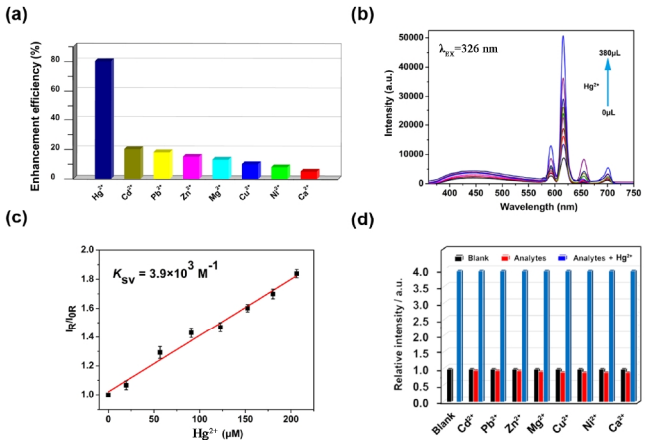

Figure 6. (a) The relative intensities for **1** dispersed in different anions aqueous solutions under 326 nm excitation. (b) Luminescent emission spectra of **1** (10^{-3} M) upon incremental addition of Hg^{2+} (10^{-3} M) under excitation at 326 nm. (c) SV plot of Hg^{2+} at lower concentrations. (d) The fluorescence emissive response of **1** for detecting Hg^{2+} in the presence of other metal ions.

Selective Sensing of Cations. Inspired by the good water stability and fluorescence properties, MOF **1** was also applied to detect different metal ions in aqueous solution. In this work, a series of metal ions including Hg^{2+}, Cd^{2+}, Pb^{2+}, Zn^{2+}, Mg^{2+}, Cu^{2+}, Ni^{2+} and Ca^{2+} were tested. The results showed that the luminescence intensity of complex **1** was influenced by different metal ions. As illustrated in Figure 6a, most metal ions in water have an inconspicuous fluorescence intensity change effect on **1**, however, the luminescence intensity of **1** was obviously increased upon the addition of Hg^{2+}.

To further study sensing ability of **1** toward Hg^{2+}, the luminescence titration experiments were performed. As demonstrated in Figure 6b, the emission intensity of **1** at 619 nm progressively enhanced with increasing the Hg^{2+} concentration. A good linear response was observed between the ratio of I_{619}/I_{467} and the concentration of Hg^{2+} (Figure 6c). Detailed analysis further revealed that the emission intensity ratio linearly varied with the Hg^{2+} concentration in low range. The K_{SV} value was 3.9 × 10^3 M^{-1} calculated by the SV plot. From the slope and standard error of the fitting line, the LOD was calculated to be 0.094 μM according to 3σ/k, which is better than those of reported luminescent sensors for Hg^{2+} detection (Table S5).

To validate the selectivity of **1** toward Hg^{2+}, the interference experiments of other metal ions were carried out. As shown in Figure 6d, the luminescence intensities of **1** changed slightly after the mere addition of other metal ions, whereas the luminescence was significantly enhanced with the introduction of Hg^{2+}, indicating that **1** could selectively and effectively sense Hg^{2+} with little interference by other cations. Aside from good selectivity, the fast response time is another crucial factor to assess sensor practicability. The fluorescence response rate of **1** to Hg^{2+} in water was measured at different time. The maximum enhancement efficiency was achieved in 30 s, and then it kept almost unchanged after 2 minutes (Figure S8). The phenomenon indicated that **1** has

Chin. J. Struct. Chem. **2022**, 41, 2211110-2211116
DOI: 10.14102/j.cnki.0254-5861.2022-0171

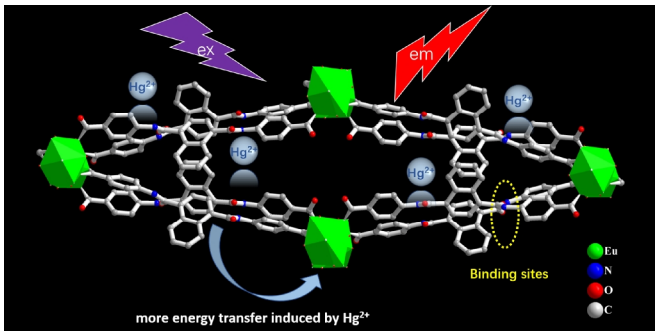

Scheme 2. Illustration of the fluorescence enhancement of MOF **1** by Hg^{2+}.

an ultrafast fluorescence response to Hg^{2+}, which is expected to be applied to real-time sensing. In addition, the luminescent MOF **1** can be continuously recollected from the solution by simple centrifugation and washing with distilled water. As shown in Figure S9, the luminescence intensities did not significantly decrease after five cycles, suggesting the excellent repeatability and reproducibility of **1** in the detection of Hg^{2+}.

The underlying mechanism of luminescence enhancement caused by Hg^{2+} was analyzed from the following aspects. First of all, as shown in Figure S6, the PXRD pattern of **1** was consistent with that of the sample after five cyclic experiments, so it can be excluded that the luminescence changing was caused by framework collapse of **1**. It is well-known that the luminescent intensity of Ln^{3+} depends on the energy transfer efficiency from the ligand to Ln^{3+} center.[39] After more efficient intramolecular energy transfer happened in MOF, Ln^{3+} can be excited more effectively and produce an enhanced fluorescence. It has been reported that the energy transfer process is more effective with the addition of certain transition metal ions.[40,43] Subsequently, the lifetime of **1** at 619 nm was increased after exposure to Hg^{2+}, which was also consistent with the trend of the luminescence intensity change (Figure S10). Therefore, an interaction may exist between Hg^{2+} and MOF, which affects the energy transfer between the ligands and Eu^{3+} centers during excitation. The intensity ratio $I_{Eu(619)}/I_{Ligand}$ of the $^5D_0/^7F_2$ line at 619 nm to that of LC emission at 467 nm is 2.3. The intensity ratio of **1** in the presence of Hg^{2+} is 6.5, indicating the energy transfer is more effective in the presence of Hg^{2+} (Figure S11). In addition, the report has shown the detection of Hg^{2+} using nitrogen because mercury ions have high affinity towards N and S atoms[44]. Therefore, the mechanism of luminescence enhancement induced by Hg^{2+} may be attributed to that the Hg^{2+} ions interact with the N atoms of acylamide groups within **1** and facilitate the efficiency of energy transformation from ligands to Eu^{3+} ions, as depicted in Scheme 2. Eventually, to confirm this hypothesis, X-ray photoelectron spectroscopy (XPS) was performed (Figure 7). The XPS data exhibit that Hg^{2+} is found after the luminescence titration experiments of **1**. The N 1s peak for **1** at 399.6 eV was shifted to 400 eV with the addition of Hg^{2+}, suggesting the coordination of Hg^{2+} with the N atoms of acylamide groups in **1**. In IR spectra, the characteristic C-N and N-H vibration bands of acylamide group are shifted from 1424 and 1659 cm^{-1} (for **1**) to 1409 and 1651 cm^{-1} (for **1** + Hg^{2+}), respectively, thus further supporting the above inference (Figure S12).

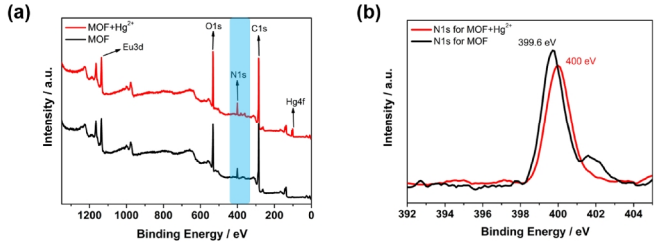

Figure 7. XPS spectra (a) and N 1s XPS (b) for MOF **1** and MOF **1** + Hg^{2+}.

n CONCLUSIONS

In conclusion, a new luminescent 3D porous Eu(III)-organic framework has been synthesized with electron-rich π-conjugated H_2L by a solvothermal method. Interestingly, this Eu-MOF showed dual luminescence and good water stability. More significantly, **1** could behave as a fast and sensitive ratiometric luminescent sensor for luminescent detection of ODZ and Hg^{2+} in water. The mechanism of fluorescence sensing was also investigated, indicating **1** can be used as an advanced sensory material for the detection of antibiotics and cations in water matrices.

n EXPERIMENTAL

Materials and General Methods. All chemicals of reagent grade were obtained from commercial sources and used without further purification. Infrared spectra were recorded on a Nicolet-5700 FT-IR spectrophotometer with KBr pellets in the 4000-400 cm^{-1} region. The powder X-ray diffraction (PXRD) patterns were recorded on an Rigaku SmartLab 9kW diffractometer with Cu Kα radiation (λ = 1.5418 Å) at room temperature. The contact angle toward water was recorded with Krüss DSA 100S instrument. The absorption spectra were recorded on a Persee T9CS UV-vis spectrophotometer. The photoluminescence spectra were measured on a Hitachi F-4700 spectrophotometer. X-ray photoelectron spectroscopy (XPS) was performed on a Thermo Fisher Scientific Escalab Xi+ system. The lifetime measurements were measured on an Edinburgh FLS 1000 Steady state, Fluorescence and Phosphorescence Lifetime Spectrometer.

Synthesis of $\{[(CH_3)_2NH_2][Eu(L)_2(H_2O)_2]\cdot xDMF\}_n$ (1). $Eu(NO_3)_3\cdot 6H_2O$ (44.6 mg, 0.1 mmol) and H_2L (45.4 mg, 0.1 mmol) were ultrasonically dissolved in 3 mL of DMF/H_2O (1:2, v/v). The mixture was sealed in a Teflon-lined stainless-steel vessel and heated at 120 ºC for 3 days. Colorless block-shaped crystals were collected. Selected IR (KBr, cm^{-1}): 3419, 1657, 1613, 1531, 1384, 1324, 1252,1179, 877 and 782.

Luminescence Sensing Experiments. Luminescence experiments of **1** toward analyte solution were recorded at room temperature. The fine-grinding sample complex **1** was dispersed in water by ultrasonication to form a uniform suspension. The titration experiments were performed by adding the selected analytes to 1 mL of **1** suspension. All titrations were carried out in triplicate to establish the consistency of the results.

X-ray Crystallography. Single-crystal X-ray diffraction data were collected on a Bruker SMART-1000 CCD diffractometer with graphite-monochromated Mo Kα (λ = 0.71073 Å) radiation at room

DOI: 10.14102/j.cnki.0254-5861.2022-0171

temperature. The structure was solved by direct methods and refined by full-matrix least-squares methods on F^2 using the SHELX-2018 program.[45] The guest $(CH_3)_2NH_2^+$ cation and solvent molecules are highly disordered. It is difficult to locate and refine the solvent peaks. Contributions to scattering due to $(CH_3)_2NH_2^+$ cation and solvent molecules were removed using the SQUEEZE routine of PLATON, and then structures were refined again using the data generated.[46] The CCDC number for complex **1** is 2190437. Crystal and refinement data are summarized in Table S1, and selected bond lengths and bond angles are listed in Table S2.

n ACKNOWLEDGEMENTS

This work was financially supported by the National Natural Science Foundation of China (No. 21771096).

n AUTHOR INFORMATION

Corresponding author. Email: zhangqingfu@lcu.edu.cn

n COMPETING INTERESTS

The authors declare no competing interests.

n ADDITIONAL INFORMATION

Supplementary information is available for this paper at http://manu30.magtech.com.cn/jghx/EN/10.14102/j.cnki.0254-5861.2022-0171

For submission: https://www.editorialmanager.com/cjschem

n REFERENCES

(1) Liu, X.; Steele, J. C.; Meng, X. Z. Usage, residue, and human health risk of antibiotics in Chinese aquaculture: a review. *Environ. Pollut*. **2017**, 223, 161-169.

(2) Wang, J. L.; Zhuan, R.; Chu, L. B. The occurrence, distribution and degradation of antibiotics by ionizing radiation: an overview. *Sci. Total Environ.* **2019**, 646, 1385-1397.

(3) Zhang, Q. Q.; Ying, G. G.; Pan, C. G.; Liu, Y. S.; Zhao, J. L. Comprehensive evaluation of antibiotics emission and fate in the river basins of China: source analysis, multimedia modeling, and linkage to bacterial resistance. *Environ. Sci. Technol*. **2015**, 49, 6772-6782.

(4) Kümmerer, K. Antibiotics in the aquatic environment - a review - part I. *Chemosphere* **2009**, 75, 417-434.

(5) Grandjean, P.; Landrigan, P. J. Developmental neurotoxicity of industrial chemicals. *Lancet* **2006**, 368, 2167-2178.

(6) Toussaint, B.; Chedin, M.; Vincent, U.; Bordin, G.; Rodriguez, A. R. Determination of (fluoro)quinolone antibiotic residues in pig kidney using liquid chromatography-tandem mass spectrometry part II: intercomparison exercise. *J. Chromatogr. A* **2005**, 1088, 40-48.

(7) Tabrizchi, M.; ILbeigi, V. Detection of explosives by positive corona discharge ion mobility spectrometry. *J. Hazard. Mater.* **2010**, 176, 692-696.

(8) Pérez-Fernández, V.; Domínguez-Vega, E.; Crego, A. L.; Ángeles García, M.; Marina, M. L. Recent advances in the analysis of antibiotics by CE and CEC. *Electrophoresis* **2012**, 33, 127-146.

(9) Cheng, Y. J.; Huang, S. H.; Singco, B.; Huang, H. Y. Analyses of sulfonamide antibiotics in meat samples by on-line concentration capillary electrochromatography-mass spectrometry. *J. Chromatogr. A* **2011**, 1218, 7640-7647.

(10) Zheng, W.; Zhou, S. Y.; Chen, Z.; Hu, P.; Liu, Y. S.; Tu, D. T.; Zhu, H. M.; Li, R. F.; Huang, M. D.; Chen, X. Y. Sub-10 nm lanthanide-doped CaF_2 nanoprobes for time-resolved luminescent biodetection. *Angew. Chem. Int. Ed*. **2013**, 52, 6671-6676.

(11) Zhang, M. R.; Zheng, W.; Liu, Y.; Huang, P.; Gong, Z. L.; Wei, J. J.; Gao, Y.; Zhou, S. Y.; Li, X. J.; Chen, X. Y. A new class of blue-LED-excitable NIR-II luminescent nanoprobes based on lanthanide-doped CaS nanoparticles. *Angew. Chem. Int. Ed*. **2019**, 58, 9556-9560.

(12) Zhang, C. G.; Zhang, M. R.; Zheng, W.; Wei, J. J.; Wang, S. T.; Huang, P.; Cheng, X. W.; Dai, T.; Chen, Z.; Chen, X. Y. A new class of luminescent nanoprobes based on main-group Sb^{3+} emitters. *Nano Res*. **2022**, 15, 179-185.

(13) Allendorf, M. D.; Bauer, C. A.; Bhakta, R. K.; Houk, R. J. T. Luminescent metal-organic frameworks. *Chem. Soc. Rev*. **2009**, 38, 1330-1352.

(14) Rasheed, T.; Nabeel, F. Luminescent metal-organic frameworks as potential sensory materials for various environmental toxic agents. *Coord. Chem. Rev.* **2019**, 401, 213065.

(15) Lu, Z. Q.; Li, Y. Z.; Hao, C.; Ru, Y.; Yang, S. J.; Zhang, N. D.; Fu, Y. Q.; Wu, W. L.; Zhou, Y. Synthesis, crystal structure and luminescent/magnetic properties of two metal-organic frameworks based on multi-N/O-donor mixed ligands. *Chin. J. Struct. Chem.* **2021**, 40, 1122-1130.

(16) Yin, Y. J.; Fang, W. J.; Liu, S. Q.; Chen, J.; Zhang, J. J.; Ni, A. Y. A new bio-metal-organic framework: synthesis, crystal structure and selectively sensing of Fe(III) Ion in aqueous medium. *Chin. J. Struct. Chem.* **2021**, 40, 1456-1460.

(17) Wang, N.; Zhou, M. S.; Li, T.; Fu, H. R.; Li, F. F. Synthesis and detection of pesticides of luminescent metal-organic framework based on carboxyl-decorating tetraphenylethylene. *Chin. J. Struct. Chem.* **2020**, 39, 1496-1502.

(18) Chen, L.; Liu, D. H.; Peng, J.; Du, Q. Z.; He, H. Ratiometric fluorescence sensing of metal-organic frameworks: tactics and perspectives. *Coord. Chem. Rev*. **2020**, 404, 213113.

(19) Yan, B. Lanthanide-functionalized metal-organic framework hybrid systems to create multiple luminescent centers for chemical sensing. *Acc. Chem. Res.* **2017**, 50, 2789-2798.

(20) Yang, L.; Song, Y. H.; Wang, L. Multi-emission metal-organic framework composites for multicomponent ratiometric fluorescence sensing: recent developments and future challenges. *J. Mater. Chem. B* **2020**, 8, 3292-3315.

(21) Yin, H. Q.; Yin, X. B. Metal-organic frameworks with multiple luminescence emissions: designs and applications. *Acc. Chem. Res.* **2020**, 53, 485-495.

(22) Wu, S. Y.; Min, H.; Shi, W.; Cheng, P. Multicenter metal-organic framework-based ratiometric fluorescent sensors. *Adv. Mater.* **2020**, 32, 1805871.

(23) (a) Li, Y.; Pang, J. D.; Bu, X. H. Multi-functional metal-organic frameworks for detection and removal of water pollutions. *Chem. Commun.* **2022**, 58, 7890-7908; (b) Yang, Y.; Pang, J. D.; Li, Y. W.; Sun, L.; Zhang, H.; Zhang, L. Y.; Xu, S. T.; Jiang, T. W. Fabrication of a stable europium-based luminescent sensor for fast detection of urinary 1-hydroxypyrene constructed from a tetracarboxylate ligand. *Inorg. Chem.* **2021**, 60, 19189-19196.

(24) Yang, Y.; Chen, L.; Jiang, F. L.; Wu, M. Y.; Pang, J. D.; Wan, X. Y.; Hong, M. C. A water-stable 3D Eu-MOF based on a metallacyclodimeric secondary building unit for sensitive fluorescent detection of acetone molecules. *CrystEngComm* **2019**, 21, 321-328.

DOI: 10.14102/j.cnki.0254-5861.2022-0171

(25) Shu, Y.; Ye, Q. Y.; Dai, T.; Xu, Q.; Hu, X. Y. Encapsulation of luminescent guests to construct luminescent metal-organic frameworks for chemical sensing. *ACS Sens*. **2021**, 6, 641-658.
(26) Zhang, X.; Hu, Q.; Xia, T. F.; Zhang, J.; Yang, Y.; Cui, Y. J.; Chen, B. L.; Qian, G. D. Turn-on and ratiometric luminescent sensing of hydrogen sulfide based on metal-organic frameworks. *ACS Appl. Mater. Interfaces* **2016**, 8, 32259-32265.
(27) Zeng, X. L.; Hu, J.; Zhang, M.; Wang, F. L.; Wu, L.; Hou, X. D. Visual detection of fluoride anions using mixed lanthanide metal-organic frameworks with a smartphone. *Anal. Chem.* **2020**, 92, 2097-2102.
(28) Yu, L.; Zheng, Q. T.; Wang, H.; Liu, C. X.; Huang, X. Q.; Xiao, Y. X. Double-color lanthanide metal-organic framework based logic device and visual ratiometric fluorescence water microsensor for solid pharmaceuticals. *Anal. Chem*. **2020**, 92, 1402-1408.
(29) (a) Alvarez, S.; Alemany, P.; Casanova, D.; Cirera, J.; Llunell, M.; Avnir, D. Shape maps and polyhedral interconversion paths in transition metal chemistry. *Coord. Chem. Rev*. **2005**, 249, 1693-1708; (b) Cirera, J.; Ruiz, E.; Alvarez, S. Shape and spin state in four-coordinate transition-metal complexes: the case of the d^6 configuration. *Chem. Eur. J*. **2006**, 12, 3162-3167.
(30) Lin, Z. J.; Yang, Z.; Liu, T. F.; Huang, Y. B.; Cao, R. Microwave-assisted synthesis of a series of lanthanide metal-organic frameworks and gas sorption properties. *Inorg. Chem*. **2012**, 51, 1813-1820.
(31) Burrows, A. D.; Cassar, K.; Düren, T.; Friend, R. M. W.; Mahon, M. F.; Rigby, S. P.; Savarese, T. L. Syntheses, structures and properties of cadmium benzenedicarboxylate metal-organic frameworks. *Dalton Trans.* **2008**, 2465-2474.
(32) Spek, A. L. Structure validation in chemical crystallography. *Acta Cryst*. **2009**, D65, 148-155.
(33) Wang, X. H.; Lei, M. Y.; Zhang, T. J.; Zhang, Q. F.; Zhang, R. F.; Yang, M. A water-stable multi-responsive luminescent Zn-MOF sensor for detecting TNP, NZF and $Cr_2O_7^{2-}$ in aqueous media. *Dalton Trans*. **2021**, 50, 3816-3824.
(34) Zhang, Q. F.; Lei, M. Y.; Kong, F.; Yang, Y. A water-stable homochiral luminescent MOF constructed from an achiral acylamide-containing dicarboxylate ligand for enantioselective sensing of penicillamine. *Chem. Commun*. **2018**, 54, 10901-10904.
(35) Hao, J. N.; Yan, B. Highly sensitive and selective fluorescent probe for Ag^+ based on a Eu^{3+} post-functionalized metal-organic framework in aqueous media. *J. Mater. Chem. A* **2014**, 2, 18018-18025.
(36) Zhang, X.; Luo, X.; Zhang, N. X.; Wu, J.; Huang, Y. Q. A highly selective and sensitive Zn(II) coordination polymer luminescent sensor for Al^{3+} and NACs in the aqueous phase. *Inorg. Chem. Front*. **2017**, 4, 1888-1894.
(37) Cho, W.; Lee, H. J.; Choi, G.; Choi, S.; Oh, M. Dual changes in conformation and optical properties of fluorophores within a metal-organic framework during framework construction and associated sensing event. *J. Am. Chem. Soc*. **2014**, 136, 12201-12204.
(38) Zhang, Q. F.; Lei, M. Y.; Yan, H.; Wang, J. Y.; Shi, Y. A water stable 3D luminescent metal-organic framework based on heterometallic $[Eu^{III}_6Zn^{II}]$ clusters showing highly sensitive, selective, and reversible detection of ronidazole. *Inorg. Chem*. **2017**, 56, 7610-7614.
(39) Arnaud, N.; Vaquer, E.; Georges, J. Comparative study of the luminescent properties of europium and terbium coordinated with thenoyltrifluoroacetone or pyridine-2,6-dicarboxylic acid in aqueous solutions. *Analyst* **1998**, 123, 261-265.
(40) Tan, H. L.; Chen, Y. Ag^+-enhanced fluorescence of lanthanide/nucleotide coordination polymers and Ag^+ sensing. *Chem. Commun*. **2011**, 47, 12373-12375.
(41) Tang, Q.; Liu, S. X.; Liu, Y. W.; Miao, J.; Li, S. J.; Zhang, L; Shi, Z.; Zheng, Z. P. Cation sensing by a luminescent metal-organic framework with multiple Lewis basic sites. *Inorg. Chem*. **2013**, 52, 2799-2801.
(42) Zhao, B.; Chen, X. Y.; Cheng, P.; Liao, D. Z.; Yan, S. P.; Jiang, Z. H. Coordination polymers containing 1D channels as selective luminescent probes. *J. Am. Chem. Soc.* **2004**, 126, 15394-15395.
(43) Hanaoka, K.; Kikuchi, K.; Kojima, H.; Urano, Y.; Nagano, T. Development of a zinc ion-selective luminescent lanthanide chemosensor for biological applications. *J. Am. Chem. Soc.* **2004**, 126, 12470-12476.
(44) Razavi, S. A. A.; Masoomi, M. Y.; Morsali, A. Double solvent sensing method for improving sensitivity and accuracy of Hg(II) detection based on different signal transduction of a tetrazine-functionalized pillared metal-organic framework. *Inorg. Chem.* **2017**, 56, 9646-9652.
(45) Sheldrick, G. M. Crystal structure refinement with SHELXL. *Acta Cryst.* **2015**, C71, 3-8.
(46) Sluis, P. V. D.; Spek, A. L. BYPASS: an effective method for the refinement of crystal structures containing disordered solvent regions. *Acta Cryst.* **1990**, A46, 194-201.

Received: July 22, 2022
Accepted: August 22, 2022
Published online: August 30, 2022
Published: October 31, 2022

DOI: 10.14102/j.cnki.0254-5861.2022-0171